

# Low-Frequency Full-Wave Finite Element Modeling Using the LU Recombination Method

H. Ke and T. H. Hubing

Department of Electrical and Computer Engineering  
Clemson University  
Clemson, SC 29634

**Abstract** – In this paper, the low-frequency instability of full-wave finite element methods (FEM) is investigated. The curl part of the FEM matrix is shown to be singular. The paper explains how low-frequency instabilities are related to this singularity. Based on this analysis, an LU recombination method is implemented in FEM to solve the low-frequency problem. This method, which has previously been applied to the method of moments (MOM), reduces the errors in the curl part of the matrix and enforces the correct gauge condition. Moreover, the method is restructured to work more efficiently for sparse finite element matrices.

## I. INTRODUCTION

The finite element method [1] is well-suited for solving problems involving inhomogeneous arbitrarily-shaped objects. Many researchers have observed that the “curl-curl” operation that is frequently employed when FEM is used to solve the vector Helmholtz equation can result in ill-conditioned matrices in some circumstances [2- 4].

One situation that generates ill-conditioned matrices and unstable solutions is modeling performed at low frequencies. The examples presented in this paper illustrate this behavior. In [5], special penalty terms were introduced and potential formulations were used to deal with this problem.

Most full-wave surface integral techniques also suffer from low frequency difficulties [6, 7]. The low frequency instabilities can be ascribed to the divergence operator applied to the unknown surface current density in the integral equation. Mathematically, these instabilities are related to the singular property of the scalar potential part of the impedance matrix. A method to circumvent this problem was recently proposed [8, 9]. This approach, called the LU recombination method, employs linear transformations of the moment matrices in order to isolate and eliminate non-physical solutions.

In this paper, the low-frequency problem with finite element formulations is described in terms of the singular property of the curl part in the finite element matrix when using curl-conforming Nedelec-type basis functions. The

LU recombination method is applied in order to isolate the singularity in the curl part of the finite element matrix. It is not necessary to introduce any penalty terms, or create new basis functions. The approach is further refined so that the new matrices after LU recombination are partially sparse. This reduces the computation cost and greatly improves the performance. Finally, a couple of examples are presented.

## II. FORMULATION

From Maxwell’s equations, the vector Helmholtz equation in terms of the  $\mathbf{E}$  field can be written as,

$$\begin{aligned} \nabla \times \left( \frac{\nabla \times \mathbf{E}(\mathbf{r})}{j\omega\mu_0\mu_r} \right) + j\omega\epsilon_0\epsilon_r\mathbf{E}(\mathbf{r}) \\ = -\mathbf{J}^{\text{int}}(\mathbf{r}) - \frac{1}{j\omega\mu_0\mu_r} \nabla \times \mathbf{M}^{\text{int}}(\mathbf{r}) \end{aligned} \quad (1)$$

where  $\mathbf{J}^{\text{int}}$  and  $\mathbf{M}^{\text{int}}$  are impressed electric and magnetic sources;  $\omega$  is the angular frequency;  $\mu_0$  and  $\epsilon_0$  are the free space permeability and permittivity; and  $\mu_r$  and  $\epsilon_r$  are the relative permeability and permittivity.

After applying a weighting function  $\mathbf{w}(\mathbf{r})$ , the FEM weak form is [4, 10],

$$\begin{aligned} \int_V \left( \frac{(\nabla \times \mathbf{E}(\mathbf{r})) \cdot (\nabla \times \mathbf{w}(\mathbf{r}))}{j\omega\mu_0\mu_r} + j\omega\epsilon_0\epsilon_r\mathbf{E}(\mathbf{r}) \cdot \mathbf{w}(\mathbf{r}) \right) dV \\ = \int_S (\hat{\mathbf{n}} \times \mathbf{H}(\mathbf{r})) \cdot \mathbf{w}(\mathbf{r}) dS - \\ \int_V \left( \mathbf{J}^{\text{int}}(\mathbf{r}) + \frac{1}{j\omega\mu_0\mu_r} \nabla \times \mathbf{M}^{\text{int}}(\mathbf{r}) \right) \cdot \mathbf{w}(\mathbf{r}) dV \end{aligned} \quad (2)$$

where  $S$  is the surface enclosing volume  $V$ .

The unknown  $\mathbf{E}$  field is expanded using curl-conforming basis functions that are the same as the weighting functions,

$$\mathbf{E}(\mathbf{r}) = \sum_n E_n \mathbf{w}_n(\mathbf{r}) \quad (3)$$

where  $E_n$  are unknown coefficients. The surface integral on the right hand side of equation (2) is evaluated by using surface basis functions  $\mathbf{f}_n(\mathbf{r})$ , which are related to  $\mathbf{w}_n(\mathbf{r})$  by,

$$\mathbf{w}_n(\mathbf{r}) = \hat{\mathbf{n}} \times \mathbf{f}_n(\mathbf{r}). \quad (4)$$

Equation (2) is then discretized into a matrix equation,

$$\mathbf{A} \cdot \mathbf{E} = \mathbf{B} \cdot \mathbf{J} + \mathbf{S}. \quad (5)$$

The right hand side represents the boundary condition and the source term.  $\mathbf{J}$  is the equivalent current density on the surface.  $\mathbf{S}$  is the source term.  $\mathbf{E}$  is a vector containing the unknown coefficients in equation (3). The elements of  $\mathbf{A}$  are,

$$A_{mn} = \int_V \left[ \frac{(\nabla \times \mathbf{w}_n(\mathbf{r})) \cdot (\nabla \times \mathbf{w}_m(\mathbf{r}))}{j\omega\mu_0\mu_r} + j\omega\varepsilon_0\varepsilon_r \mathbf{w}_n(\mathbf{r}) \cdot \mathbf{w}_m(\mathbf{r}) \right] dV. \quad (6)$$

Let

$$A_{1mn} = \int_V j\omega\varepsilon_0\varepsilon_r \mathbf{w}_n(\mathbf{r}) \cdot \mathbf{w}_m(\mathbf{r}) dV, \quad (7a)$$

which is the right-most term in the right-hand side of equation (6).

Let

$$A_{2mn} = \int_V \frac{(\nabla \times \mathbf{w}_n(\mathbf{r})) \cdot (\nabla \times \mathbf{w}_m(\mathbf{r}))}{j\omega\mu_0\mu_r} dV, \quad (7b)$$

which is the left-most term in the right-hand side of equation (6). Every element of  $\mathbf{A}_1$  approaches zero at arbitrarily low frequencies. The following reasoning demonstrates that, because of the  $\nabla \times$  operator,  $\mathbf{A}_2$  is a singular matrix when using the popular lowest order curl-conforming basis functions. The rank of the matrix is determined by the total number of internal nodes in the finite element mesh [11].

The basis function for a tetrahedron can be defined on each edge as [12],

$$\mathbf{w}_{7-i} = \begin{cases} \mathbf{f}_{7-i} + \mathbf{g}_{7-i} \times \mathbf{r} & \mathbf{r} \text{ in the tetrahedra} \\ 0 & \text{otherwise} \end{cases} \quad (8a)$$

$i = 1, 2, \dots, 6$

where

$$\mathbf{f}_{7-i} = \frac{l_{7-i}}{6V} \mathbf{r}_{i1} \times \mathbf{r}_{i2}, \quad (8b)$$

and

$$\mathbf{g}_{7-i} = \frac{l_i l_{7-i}}{6V} \mathbf{e}_i. \quad (8c)$$

Here  $i_1$  and  $i_2$  are the node indices of edge  $i$ , defined in Fig. 1.  $l$  is the length of the edge,  $\mathbf{e}$  is the unit vector along the edge, and  $V$  is the volume of the tetrahedron.

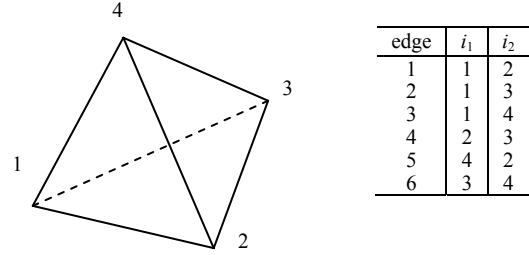


Fig. 1. The tetrahedral element and its edge-node relations.

Consider the local elements, i.e., the elements evaluated within one tetrahedron. The curl of the basis function is a constant within the tetrahedron,

$$\nabla \times \mathbf{w}_i = 2\mathbf{g}_i = \frac{l_i}{6V} \mathbf{l}_{7-i}. \quad (9)$$

The local element in  $\mathbf{A}_2^e$  is,

$$\begin{aligned} A_{2ij}^e &= \frac{1}{j\omega\mu_0\mu_r} 4\mathbf{g}_i \cdot \mathbf{g}_j V \\ &= \frac{1}{j\omega\mu_0\mu_r} \left( \frac{l_i l_j}{9V} \mathbf{l}_i \cdot \mathbf{l}_j \right) \end{aligned} \quad (10)$$

where the superscript  $e$  indicates local elements. Thus within one tetrahedron, the local matrix can be written as in equation (11), shown on the top of the next page.

For the tetrahedron in Fig. 1, edges 4, 5, and 6 form a triangle, which means,

$$\mathbf{l}_4 + \mathbf{l}_5 + \mathbf{l}_6 = 0. \quad (12)$$

Consequently, the first three rows in equation (11) are linearly dependent.

$$\mathbf{A}_2^e = \frac{1}{j\omega\mu_0\mu_r} \begin{bmatrix} \frac{l_1 l_1}{9V} \mathbf{l}_6 \cdot \mathbf{l}_6 & \frac{l_1 l_2}{9V} \mathbf{l}_6 \cdot \mathbf{l}_5 & \frac{l_1 l_3}{9V} \mathbf{l}_6 \cdot \mathbf{l}_4 & \frac{l_1 l_4}{9V} \mathbf{l}_6 \cdot \mathbf{l}_3 & \frac{l_1 l_5}{9V} \mathbf{l}_6 \cdot \mathbf{l}_2 & \frac{l_1 l_6}{9V} \mathbf{l}_6 \cdot \mathbf{l}_1 \\ \frac{l_2 l_1}{9V} \mathbf{l}_5 \cdot \mathbf{l}_6 & \frac{l_2 l_2}{9V} \mathbf{l}_5 \cdot \mathbf{l}_5 & \frac{l_2 l_3}{9V} \mathbf{l}_5 \cdot \mathbf{l}_4 & \frac{l_2 l_4}{9V} \mathbf{l}_5 \cdot \mathbf{l}_3 & \frac{l_2 l_5}{9V} \mathbf{l}_5 \cdot \mathbf{l}_2 & \frac{l_2 l_6}{9V} \mathbf{l}_5 \cdot \mathbf{l}_1 \\ \frac{l_3 l_1}{9V} \mathbf{l}_4 \cdot \mathbf{l}_6 & \frac{l_3 l_2}{9V} \mathbf{l}_4 \cdot \mathbf{l}_5 & \frac{l_3 l_3}{9V} \mathbf{l}_4 \cdot \mathbf{l}_4 & \frac{l_3 l_4}{9V} \mathbf{l}_4 \cdot \mathbf{l}_3 & \frac{l_3 l_5}{9V} \mathbf{l}_4 \cdot \mathbf{l}_2 & \frac{l_3 l_6}{9V} \mathbf{l}_4 \cdot \mathbf{l}_1 \\ \frac{l_4 l_1}{9V} \mathbf{l}_3 \cdot \mathbf{l}_6 & \frac{l_4 l_2}{9V} \mathbf{l}_3 \cdot \mathbf{l}_5 & \frac{l_4 l_3}{9V} \mathbf{l}_3 \cdot \mathbf{l}_4 & \frac{l_4 l_4}{9V} \mathbf{l}_3 \cdot \mathbf{l}_3 & \frac{l_4 l_5}{9V} \mathbf{l}_3 \cdot \mathbf{l}_2 & \frac{l_4 l_6}{9V} \mathbf{l}_3 \cdot \mathbf{l}_1 \\ \frac{l_5 l_1}{9V} \mathbf{l}_2 \cdot \mathbf{l}_6 & \frac{l_5 l_2}{9V} \mathbf{l}_2 \cdot \mathbf{l}_5 & \frac{l_5 l_3}{9V} \mathbf{l}_2 \cdot \mathbf{l}_4 & \frac{l_5 l_4}{9V} \mathbf{l}_2 \cdot \mathbf{l}_3 & \frac{l_5 l_5}{9V} \mathbf{l}_2 \cdot \mathbf{l}_2 & \frac{l_5 l_6}{9V} \mathbf{l}_2 \cdot \mathbf{l}_1 \\ \frac{l_6 l_1}{9V} \mathbf{l}_1 \cdot \mathbf{l}_6 & \frac{l_6 l_2}{9V} \mathbf{l}_1 \cdot \mathbf{l}_5 & \frac{l_6 l_3}{9V} \mathbf{l}_1 \cdot \mathbf{l}_4 & \frac{l_6 l_4}{9V} \mathbf{l}_1 \cdot \mathbf{l}_3 & \frac{l_6 l_5}{9V} \mathbf{l}_1 \cdot \mathbf{l}_2 & \frac{l_6 l_6}{9V} \mathbf{l}_1 \cdot \mathbf{l}_1 \end{bmatrix} \quad (11)$$

Or more specifically, consider the normalized local matrix  $(\mathbf{A}_2^e)^N$  whose elements are given by,

$$(\mathbf{A}_{2ij}^e)^N = \frac{1}{j\omega\mu_0\mu_r} \left( \frac{1}{9V} \mathbf{l}_i \cdot \mathbf{l}_j \right) = \frac{1}{l_i l_j} A_{2ij}^e. \quad (13)$$

The first three rows of  $(\mathbf{A}_2^e)^N$  are linearly dependent and are related by integers,

$$\begin{aligned} (A_{21j}^e)^N + (A_{22j}^e)^N + (A_{23j}^e)^N &= 0 \\ j &= 1, 2, \dots, 6 \end{aligned} \quad (14)$$

This relationship is similar to equation (11) in [9]. The linearly dependent rows correspond to the edges in the tetrahedron sharing a common node. After assembling the local matrices into a global matrix, the rows of the global matrix corresponding to edges sharing the same nodes are linearly dependent, resulting in a singular global  $\mathbf{A}_2$ .

It is evident from equation (7) that the FEM matrix ( $\mathbf{A} = \mathbf{A}_1 + \mathbf{A}_2$ ) will be unstable at low frequencies, since a matrix ( $\mathbf{A}_1$ ) with elements approaching zero will be added to a singular matrix ( $\mathbf{A}_2$ ). Due to limited computer precision, the elements of  $\mathbf{A}_1$  can become buried in the round-off error and not even affect the values in the overall finite element matrix. However, the information in  $\mathbf{A}_1$  incorporates the gauge condition for the electric field [5]. Without this information, the matrix equation (5) is ill-conditioned, resulting in significant errors in the solution.

### III. LU RECOMBINATION METHOD IN FEM

Based on the above analysis, the low frequency problem in FEM is analogous to the low-frequency problem in the boundary element method [9]. Consequently, the LU recombination method developed for the boundary element method can be applied to the finite element method. LU recombination can be used to enforce the singular property of  $\mathbf{A}_2$  and preserve the correct gauge condition in matrix  $\mathbf{A}_1$ . However, the original  $\mathbf{A}_2$  is a sparse matrix. Applying LU recombination in the manner described in [9] would produce a new, dense  $\mathbf{A}_2$  matrix. This would be highly undesirable in an FEM formulation. Therefore, an incomplete LU recombination technique that is suitable for sparse matrices was developed. In this approach, only part of  $\mathbf{A}_2$  is modified and the resulting new matrix is still sparse. The sparseness of the new matrix depends on the number of inner nodes in the mesh.

The method begins with the L-D-U decomposition of  $\mathbf{A}_2$ , shown in equation (15) at the bottom of this page, just as it does when applied to the boundary element method [9],

$$\begin{aligned} \begin{bmatrix} \mathbf{A}_{2ii} & \mathbf{A}_{2id} \\ \mathbf{A}_{2di} & \mathbf{A}_{2dd} \end{bmatrix} &= \begin{bmatrix} \mathbf{L}_{ii} & \mathbf{0} \\ \mathbf{L}_{di} & \mathbf{L}_{dd} \end{bmatrix} \cdot \begin{bmatrix} \mathbf{U}_{ii} & \mathbf{U}_{id} \\ \mathbf{U}_{di} & \mathbf{U}_{dd} \end{bmatrix} \\ &= \begin{bmatrix} \mathbf{L}_{ii} & \mathbf{0} \\ \mathbf{L}_{di} & \mathbf{L}_{dd} \end{bmatrix} \cdot \begin{bmatrix} \mathbf{D}_{2ii} & \mathbf{D}_{2id} \\ \mathbf{D}_{2di} & \mathbf{D}_{2dd} \end{bmatrix} \cdot \begin{bmatrix} \mathbf{L}_{ii} & \mathbf{0} \\ \mathbf{L}_{di} & \mathbf{L}_{dd} \end{bmatrix}^T. \end{aligned} \quad (15)$$

The  $\mathbf{A}_2$  matrix is partitioned so that the linearly independent rows (represented by the subscript  $ii$ ) are grouped together and the dependent rows (subscript  $dd$ ) are moved to the end. The LU recombination method will

modify the sub-matrices  $\mathbf{L}_{di}$ ,  $\mathbf{D}_{2di}$ ,  $\mathbf{D}_{2id}$ , and  $\mathbf{D}_{2dd}$ , while  $\mathbf{L}_{ii}$  and  $\mathbf{D}_{2ii}$  are left unchanged. Therefore,  $\mathbf{A}_{2ii}=\mathbf{L}_{ii}\cdot\mathbf{D}_{2ii}$  is unchanged after constructing a new  $\mathbf{A}_2$ . There is no need to recalculate  $\mathbf{A}_{2ii}$  after the modifications on  $\mathbf{L}$  and  $\mathbf{D}_2$ . To accomplish that, the  $\mathbf{L}$  matrix is replaced by,

$$\mathbf{L} = \begin{bmatrix} \mathbf{I}_{ii} & \mathbf{0} \\ \mathbf{L}_{di} & \mathbf{I}_{dd} \end{bmatrix}, \quad (16)$$

where  $\mathbf{I}$  is identity matrix. The new decomposition on  $\mathbf{A}_2$  is then written in equation (17), as shown at the bottom of this page. Thus during the LU recombination, the  $\mathbf{A}_{2ii}$  part remains the same. No additional elements or errors are introduced.

The same decomposition in equation (17) is applied to  $\mathbf{A}_1$ . After LU recombination, the new  $\mathbf{A}$  becomes equation (18) at the bottom of this page. Note that  $\mathbf{L}_{di}$  is already modified, as described in [9]. The correct information in  $\mathbf{A}_1$  is preserved. But the new  $\mathbf{A}$  matrix is still ill-conditioned at low frequencies since  $\mathbf{A}_1$  is much smaller than  $\mathbf{A}_2$ . The imbalance can be alleviated by introducing a scaling step. The sub-matrices  $\mathbf{D}_{1di}$ ,  $\mathbf{D}_{1id}$ , and  $\mathbf{D}_{1dd}$  are scaled so that they are comparable to  $\mathbf{A}_{2ii}$ . This step greatly improves the condition of the new  $\mathbf{A}$  matrix. It is especially beneficial when iterative methods are used to solve the matrix equations.

#### IV. NUMERICAL RESULTS

Two sample structures were evaluated using a finite element modeling technique with and without LU recombination. The first example is the rectangular power bus structure shown in Fig. 2. The dimensions of the structure are 20 cm x 20 cm x 1 cm. The power and ground planes are modeled as perfect electric conductors (PECs). The four side walls of the board are modeled as perfect magnetic conductors (PMCs). The dielectric between the planes has a relative permittivity of 4.5. The board is excited by an ideal current source located in the dielectric, 6 cm from one edge and 7 cm from an adjacent edge.

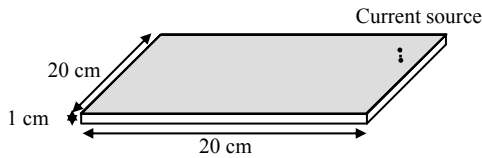


Fig. 2. A power bus example.

The input impedance of the power bus was calculated, and the results obtained using different methods are shown in Fig. 3. The solid dots show the result obtained using the standard FEM formulation. This

technique fails when the frequency is below 1 MHz. The lower frequency limit is determined by the number of significant figures used when manipulating the elements of the FEM matrix. The solid line indicates the result when the LU recombination method is incorporated into the FEM. This result is accurate even below a few Hz.

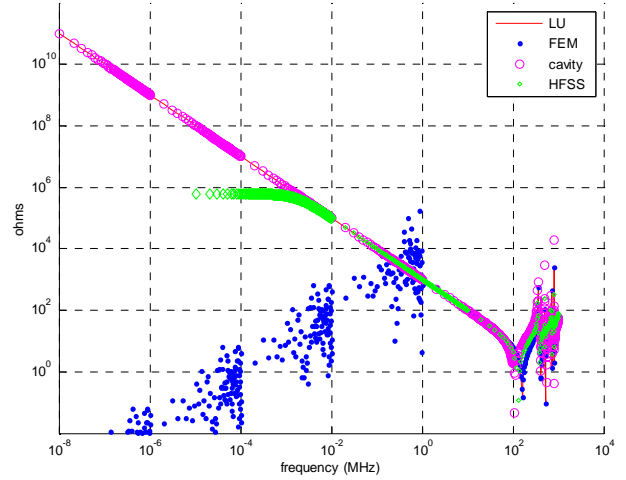


Fig. 3. The input impedance of the power bus.

Also shown in Fig. 3 are the results calculated using a cavity model and Ansoft HFSS [13]. The cavity model is a mode-expansion method suitable for rectangular power bus geometries. It models the power bus as a  $\text{TM}_z$  cavity and determines the input impedance by summing the contributions of all relevant resonant modes [14]. This method has no problem at low frequencies but it can be difficult to apply to complicated geometries. HFSS, which is a FEM modeling code, extrapolates from the high frequency results to obtain a low frequency approximation. In this case, the extrapolation was valid down to a few kHz.

$$\begin{bmatrix} \mathbf{A}_{2ii} & \mathbf{A}_{2id} \\ \mathbf{A}_{2di} & \mathbf{A}_{2dd} \end{bmatrix} = \begin{bmatrix} \mathbf{I}_{ii} & \mathbf{0} \\ \mathbf{L}_{di} & \mathbf{I}_{dd} \end{bmatrix} \cdot \begin{bmatrix} \mathbf{A}_{ii} & \mathbf{A}_{id} \\ \mathbf{U}_{di} & \mathbf{U}_{dd} \end{bmatrix} \quad (17)$$

$$= \begin{bmatrix} \mathbf{I}_{ii} & \mathbf{0} \\ \mathbf{L}_{di} & \mathbf{I}_{dd} \end{bmatrix} \cdot \begin{bmatrix} \mathbf{A}_{2ii} & \mathbf{D}_{2id} \\ \mathbf{D}_{2di} & \mathbf{D}_{2dd} \end{bmatrix} \cdot \begin{bmatrix} \mathbf{I}_{ii} & \mathbf{0} \\ \mathbf{L}_{di} & \mathbf{I}_{dd} \end{bmatrix}^T$$

$$\begin{bmatrix} \mathbf{A}_{ii} & \mathbf{A}_{id} \\ \mathbf{A}_{di} & \mathbf{A}_{dd} \end{bmatrix} = \begin{bmatrix} \mathbf{I}_{ii} & \mathbf{0} \\ \tilde{\mathbf{L}}_{di} & \mathbf{I}_{dd} \end{bmatrix} \cdot \quad (18)$$

$$\left( \begin{bmatrix} \mathbf{A}_{1ii} & \mathbf{D}_{1id} \\ \mathbf{D}_{1di} & \mathbf{D}_{1dd} \end{bmatrix} + \begin{bmatrix} \mathbf{A}_{2ii} & \mathbf{0} \\ \mathbf{0} & \mathbf{0} \end{bmatrix} \right) \cdot \begin{bmatrix} \mathbf{I}_{ii} & \mathbf{0} \\ \tilde{\mathbf{L}}_{di} & \mathbf{I}_{dd} \end{bmatrix}^T$$

The second example is a stripline structure consisting of a metal trace imbedded in a dielectric between two metal planes as shown in Fig. 4. The dimensions of the planes are 20 mm x 10 mm and they are 2 mm apart. The dielectric constant is 4.5. The trace has a width of 1 mm and a length of 10 mm. The trace is driven by a 0.1-A current source at one end, and is terminated by a 50- $\Omega$  resistor on the other end. In this example the top and bottom planes are modeled as PECs, and the equivalent current on the dielectric boundary is set to zero. Also shown in Fig. 4 is the top view of the FEM mesh.

Figure 5 shows the magnitude of the input impedance calculated at the source port. The impedance should have a real value of 50  $\Omega$  at low frequencies. The regular FEM result exhibits significant errors below 1 MHz. In fact, there are observable instability problems at frequencies above 1 MHz. With the help of the LU recombination method, the error is corrected and the results are accurate down to a few Hz.

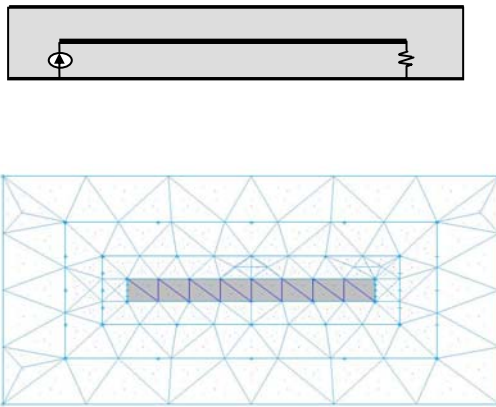


Fig. 4. A microstrip example and the mesh.

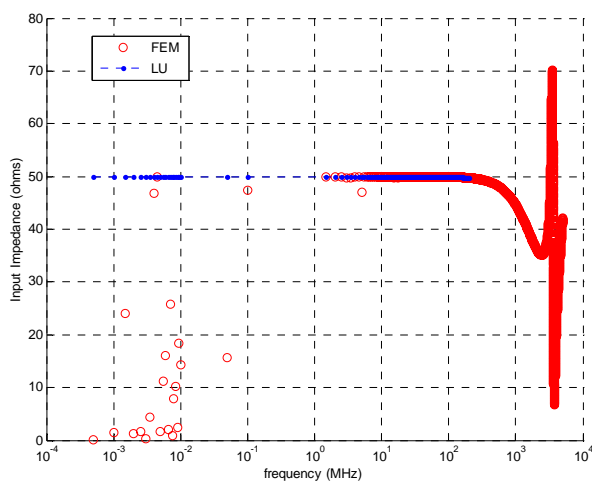


Fig. 5. The input impedance of the stripline

## V. CONCLUSION

The singular behavior of the discretized curl term in the vector Helmholtz equation causes low-frequency instabilities in full-wave FEM formulations. The LU recombination method can be applied to existing FEM codes to solve this problem. The LU recombination method uses linear transformations to minimize the influence of errors in the curl part of the matrix. Properly applied, it is possible to preserve the sparseness of the FEM matrix.

## REFERENCES

- [1] J. Jin, *The Finite Element Method in Electromagnetics*, New York: John Wiley & Sons Inc., 1993.
- [2] W. Boyse, G. Minerbo, K. Paulsen, and D. Lynch, "Application of potentials to finite element modeling of Maxwell's equations," *IEEE Trans. Magn.*, vol. 29, no. 2, pp. 1333-1336, Mar. 1993.
- [3] J. Lee, D. Sun, and Z. Cendes, "Tangential vector finite elements for electromagnetic field computation," *IEEE Trans. Magn.*, vol. 27, pp. 4032-4035, Sep. 1991.
- [4] A. F. Peterson, S. L. Ray, and R. Mittra, *Computational Methods for Electromagnetics*, pp. 461-463, New York: IEEE Press and Oxford University Press, 1997.
- [5] R. Dyczij-Edlinger, G. Peng, and J. Lee, "Efficient finite element solvers for the Maxwell equations in the frequency domain," *Computer Methods in Applied Mechanics and Engineering*, vol. 169, no. 3, pp. 297-309, Feb. 1999.
- [6] M. Burton and S. Kashyap, "A study of a recent, moment-method algorithm that is accurate to very low frequencies," *Appl. Computational Electromagn. Soc. J.*, vol. 10, no. 3, pp. 58-68, Nov. 1995.
- [7] W. Wu, A. W. Glisson, and D. Kajfez, "A study of two numerical solution procedures for the electric field integral equation at low frequency," *Appl. Computational Electromagn. Soc. J.*, vol. 10, no. 3, pp. 69-80, Nov. 1995.
- [8] H. Ke and T. Hubing, "Using an LU recombination method to improve the performance of the boundary element method at very low frequencies," *Proceedings of the 2005 IEEE Int. Symp. On EMC*, Chicago, IL, Aug. 2005.
- [9] H. Ke and T. Hubing, "A modified LU recombination technique for improving the performance of boundary element methods at low frequencies," *Appl. Computational Electromagn. Soc. J.*, vol. 20, no. 3, pp. 178-185, Nov. 2005.
- [10] Y. Ji, "Development and applications of a hybrid finite-element-method/method-of-moments ( FEM / MOM) tool to model electromagnetic compatibility

and signal integrity problems in printed circuit boards,” Ph.D. dissertation, University of Missouri-Rolla, 2000.

- [11] N. Venkatarayalu, M. Vouvakis, Y. Gan, and J. Lee, “Suppressing linear time growth in edge element based finite element time domain solution using divergence free constraint equation,” *IEEE Antennas and Propagation Society International Symposium*, vol. 4b, pp. 193-196, Jul. 2005.
- [12] X. Yuan, “Three-dimensional electromagnetic scattering from inhomogeneous objects by the hybrid moment and finite element method,” *IEEE Trans. Microwave Theory and Tech.*, vol. 38, no. 8, pp. 1053-1058, Aug. 1990.
- [13] HFSS version 9.0, Ansoft Corporation. <http://www.ansoft.com/products/hf/hfss/>
- [14] M. Xu and T. Hubing, “Estimating the power bus impedance of printed circuit boards with embedded capacitance,” *IEEE Trans. Adv. Packag.*, vol. 25, no. 3, pp. 424-432, Aug. 2002.



**Haixin Ke** received his BSEE and MSEE degrees from Tsinghua University in 1998 and 2001, respectively, and his Ph.D. in Electrical Engineering from University of Missouri-Rolla in 2006. He is currently a Post-Doctoral researcher at Clemson University. His research

interests include computational electromagnetics, electromagnetic compatibility, and vehicular electronic systems.



**Todd Hubing** received his BSEE degree from the Massachusetts Institute of Technology in 1980, his MSEE degree from Purdue University in 1982, and his Ph.D. in Electrical Engineering from North Carolina State University in 1988. From 1982 to 1989, he was employed in the Electromagnetic Compatibility Laboratory, IBM Communications Products Division, in Research Triangle Park, NC. In 1989, he joined faculty at the University of Missouri-Rolla (UMR). At UMR, he worked with faculty and students to analyze and develop solutions for a wide range of EMC problems affecting the electronics industry. In 2006, he joined Clemson University as the Michelin Professor for Vehicular Electronics. There he is continuing his work in electromagnetic compatibility and computational electromagnetic modeling, particularly as it is applied to automotive and aerospace electronic designs. Prof. Hubing has served as an associate editor of the IEEE Transactions on EMC, the IEEE EMC Society Newsletter, and the Journal of the Applied Computational Electromagnetics Society. He has served on the board of directors for both the Applied Computational Electromagnetics Society and the IEEE EMC Society. He was the 2002-2003 President of the IEEE EMC Society and is a Fellow of the IEEE.